Supplementary Information (SI) for Journal of Materials Chemistry A.
This journal is © The Royal Society of Chemistry 2024

Supplementary Material

Construction of a cobalt-doped Ni_3S_2@NiFe-LDH heterojunction with enhanced local electric field for efficient oxygen evolution reaction

Jie Wu,[‡a] Anqi Huang,[‡a] Wen Cao,[a] Xuehui Gao,[a*] Zhongwei Chen[b, c*]

[a] Key Laboratory of the Ministry of Education for Advanced Catalysis Material, College of Chemistry and Materials Science, Zhejiang Normal University, Jinhua 321004, China.

[b] State Key Laboratory of Catalysis-Energy, Dalian Institute of Chemical Physics, Chinese Academy of Sciences, Dalian, 116023 P. R. China.

[c] Power Battery and Systems Research Center, Dalian Institute of Chemical Physics, Chinese Academy of Sciences, Dalian 116023, China.

Computational and experimental details

Computational details

All computations were carried out within the density functional theory framework, employing the projector augmented wave method as realized in the Vienna Ab Initio Simulation Package (VASP)[1]. We employed the Generalized Gradient Approximation (GGA), specifically utilizing the Perdew-Burke-Ernzerhof (PBE) functional, [2] and incorporated Hubbard U corrections (with values of 5.3 eV for Fe, 3.6 eV for Co, and 6.4 eV for Ni 3d orbitals) to account for the self-interaction errors inherent in transition metal calculations. Additionally, a plane-wave cutoff energy of 500 eV was adopted to ensure computational precision. The van der The van der Waals interactions were accounted for using the DFT-D3 correction method. A perpendicular vacuum spacing of 15 Å was included to prevent spurious interactions between periodic replicas of the structure. For the Brillouin zone integration, a 2×2×1 k-point mesh was employed to ensure sufficient sampling. All atomic configurations underwent relaxation until the residual forces acting on each atom diminished to below 0.01 eV/Å, thus achieving a structurally stable state.

Materials synthesis

Synthesis of NiCo-PBA:

NiCo-PBA nanocubes were fabricated through a straightforward room-temperature aging process. The synthesis began with dissolving 2.647 g of $Na_3C_6H_5O_7 \cdot 2H_2O$ and 1.426 g of $NiCl_2 \cdot 6H_2O$ in 200 mL of deionized (DI) water to constitute Solution A. Concurrently, 1.320 g of $K_3[Co(CN)_6]$ was dissolved in another 200 mL of DI water to prepare Solution B. Following complete dissolution of both components, pour solution B into solution A and stir quickly for 10 minutes, subsequently stand undisturbed for 48 hours at ambient conditions to facilitate nanocubes growth. Post-aging, the mixture underwent centrifugation for solid-liquid

separation, followed by retrieval of the precipitate. The harvested product was rinsed with DI water and ethanol to remove any residual impurities, and finally dried in an oven maintained at 60 ℃ to obtain the purified NiCo-PBA nanocubes.

Synthesis of Co-Ni_3S_2:

20 mg of NiCo-PBA powder obtained in the aforementioned steps was dissolved in 20 mL absolute ethanol to compose Solution A. Meanwhile, 40 g of Na_2S were dissolved in 10 mL of DI water to create Solution B. After sufficient dissolution, Solution B was introduced into Solution A under stirring, yielding a uniform mixture. This blend was then introduced into a 50 mL Teflon-coated stainless steel autoclave, where it was heated to 100 ℃ for a duration of 250 minutes. Post-reaction, the resultant materials were isolated via centrifugation, rinsed with DI water and ethanol to ensure purity, and finally dried at 60 ℃ for 12 hours. The resultant substance from this process was designated as Co-Ni_3S_2.

Synthesis of Co-Ni_3S_2@NiFe-LDH:

60 mg of Co-Ni_3S_2, 0.6 g of urea and 0.6 g of polyvinylpyrrolidone (PVP) was dispersed in 60 mL of DI water while stirring for 15 min. After that, 120 mg of Ni $(NO_3)_2 \cdot 6H_2O$ and 38.24 mg of $FeSO_4 \cdot 7H_2O$ were added successively and stirring for an additional 30 min. Subsequently, the solution was then subjected to heat in an oil bath maintained at 90 °C for 4 hours under reflux conditions. Post-heating, the product was washed multiple times with DI water and ethanol to remove any impurities. Lastly, the material was dried in an oven at 60 ℃ for 12 hours, culminating in the synthesis of Co-Ni_3S_2@NiFe-LDH. NiFe-LDH was synthesized by the same method but without the introduction of Co-Ni_3S_2.

Fabrication of working electrodes:

To prepare the nickel foam (NF) substrate, a piece measuring 1*1.5 cm^2 underwent intense ultrasonic cleaning in a 3 M HCl solution for about 30 minutes. This step was crucial to eliminate the surface oxide layer

and any contaminants. Afterwards, the NF was thoroughly rinsed with DI water until the rinse water reached a neutral pH value, roughly 7, indicating the removal of acidic residues. The cleaned NF was then dried thoroughly in a vacuum oven at 80 °C overnight. The catalyst, Super P (conductive carbon black), and polyvinylidene fluoride (PVDF) were combined in a mass ratio of 7:2:1. This blend was ground to achieve a homogeneous mixture. Next, 230 uL of N-Methyl-2-pyrrolidone (NMP) was added to the mixture, which was then stirred until a consistent ink-like dispersion was formed. This ink was carefully applied over a 1×1 cm^2 area of the pretreated NF, with a targeted loading density of approximately 2.0 mg cm^{-2}. The ink-coated NF was ultimately dried in a vacuum oven at 80 °C overnight.

Electrochemical measurements:

Measurements of an electrochemical performance were executed utilizing a CHI760E workstation from CH Instruments, deploying a conventional three-electrode configuration submerged in a 1.0 M KOH medium. Herein, the working electrode was fabricated adhering to the aforementioned procedure, accompanied by a Hg/HgO electrode serving as the reference and a graphite rod acting as the counter electrode. All recorded potential values were adjusted to reference the Reversible Hydrogen Electrode (RHE), in accordance with the Nernst equation: $E_{RHE} = E_{Hg/Hgo} + 0.059pH + 0.098$, unless explicitly stated otherwise. Linear Sweep Voltammetry (LSV) profiles were attained at a scan rate of 5 mV s^{-1} from 1.003 to 1.803 V vs. RHE, with 90% internal resistance (iR) compensation. The overpotential (η) was determined using the formula: $\eta = E_{RHE} - 1.23\ V - iR$. Tafel slopes were obtained by fitting linear portions from LSV. Electrochemical Impedance Spectroscopy (EIS) measurements were conducted with an amplitude signal of 5 mV, sweeping frequencies extensively from 100 kHz down to 0.1 Hz. The double-layer capacitance (C_{dl}) was derived from the capacitive current data points captured at the midpoint potential across various scan rates. The slope of this

line directly corresponds to the value of C_{dl}. To assess the long-term stability, a 40-hour continuous chronoamperometric test was conducted at a constant current density of 10 mA cm^{-2}.

Characterization:

The surface morphology and microstructural features of the samples were examined using both a Scanning Electron Microscope (SEM; model Hitachi S-4800) and a Transmission Electron Microscope (TEM; model JEM-2100F) to ensure comprehensive visualization. The crystalline structures of the catalyst materials were analyzed through X-ray Powder Diffraction (XRD) measurements employing a state-of-the-art D8 Advance X-ray Diffractometer from Bruker AXS. Surface chemical states were investigated utilizing X-ray Photoelectron Spectroscopy (XPS) with an ESCALAB-250Xi instrument. Ultraviolet Photoelectron Spectroscopy (UPS) measurements were carried out using the advanced Thermo ESCALAB 250XI system to elucidate the electronic structure and energy levels at the material's surface. Ultraviolet visible near infrared (UV-Vis-NIR) spectrophotometer were characterized on Cary 5000. Raman spectroscopy was collected on Renishaw RM1000 Raman spectroscopy (Hong Kong) using the 532 nm laser line.

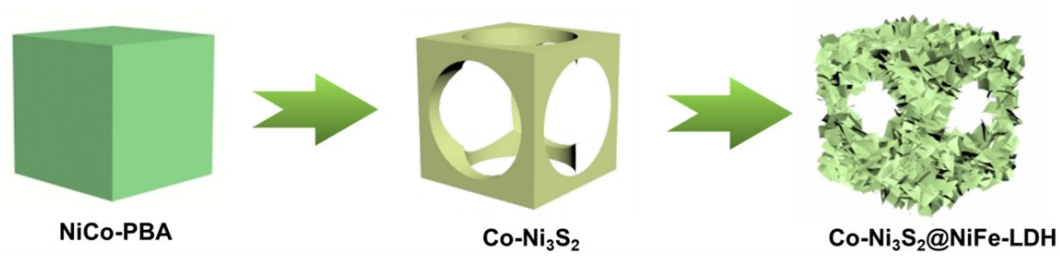

Fig. S1. Scheme of the preparation of Co-Ni_3S_2@NiFe-LDH.

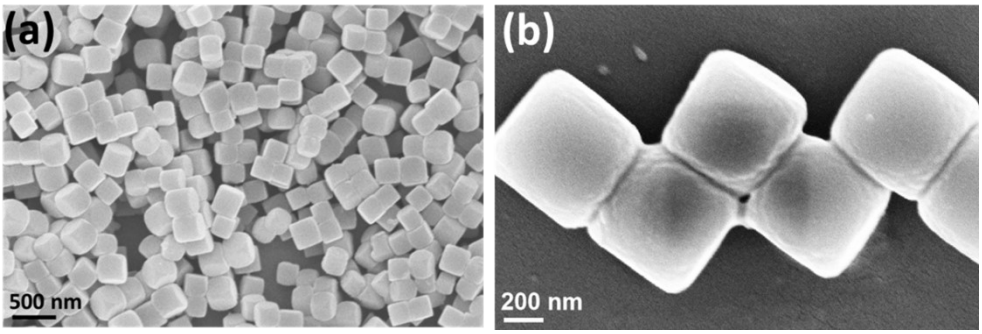

Fig. S2. SEM images of NiCo-PBA.

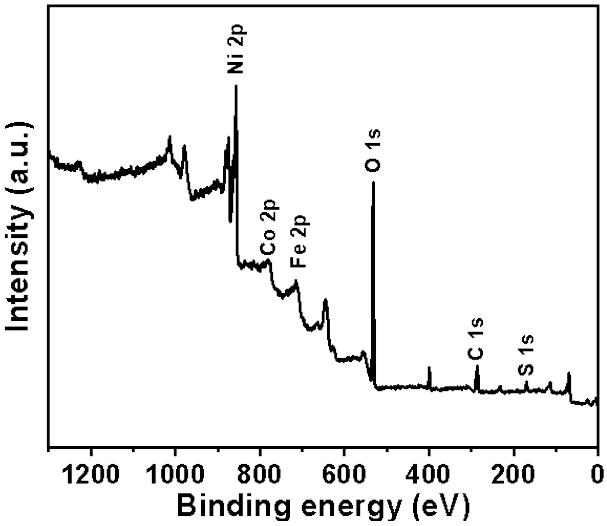

Fig. S3. XPS survey spectrum of Co-Ni_3S_2@NiFe-LDH.

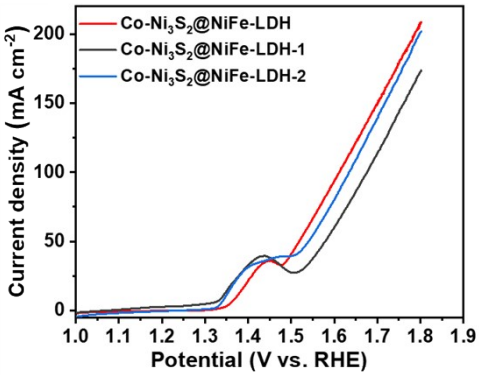

Fig. S4. LSV curves of Co-Ni_3S_2@NiFe-LDH, Co-Ni_3S_2@NiFe-LDH-1 and Co-Ni_3S_2@NiFe-LDH-2 without IR compensation.

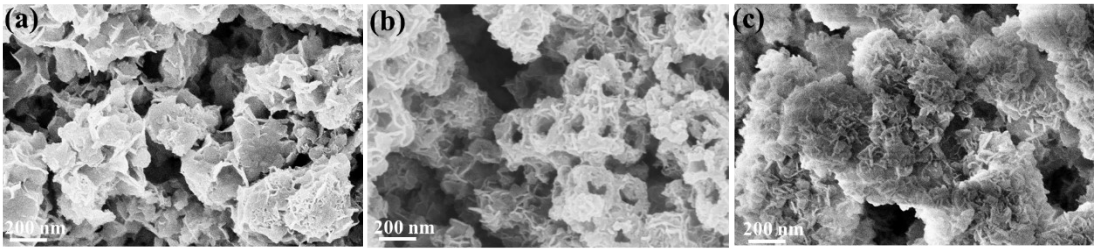

Fig. S5 SEM images of (a) Co-Ni_3S_2@NiFe-LDH-1, Co-Ni_3S_2@NiFe-LDH and Co-Ni_3S_2@NiFe-LDH-2

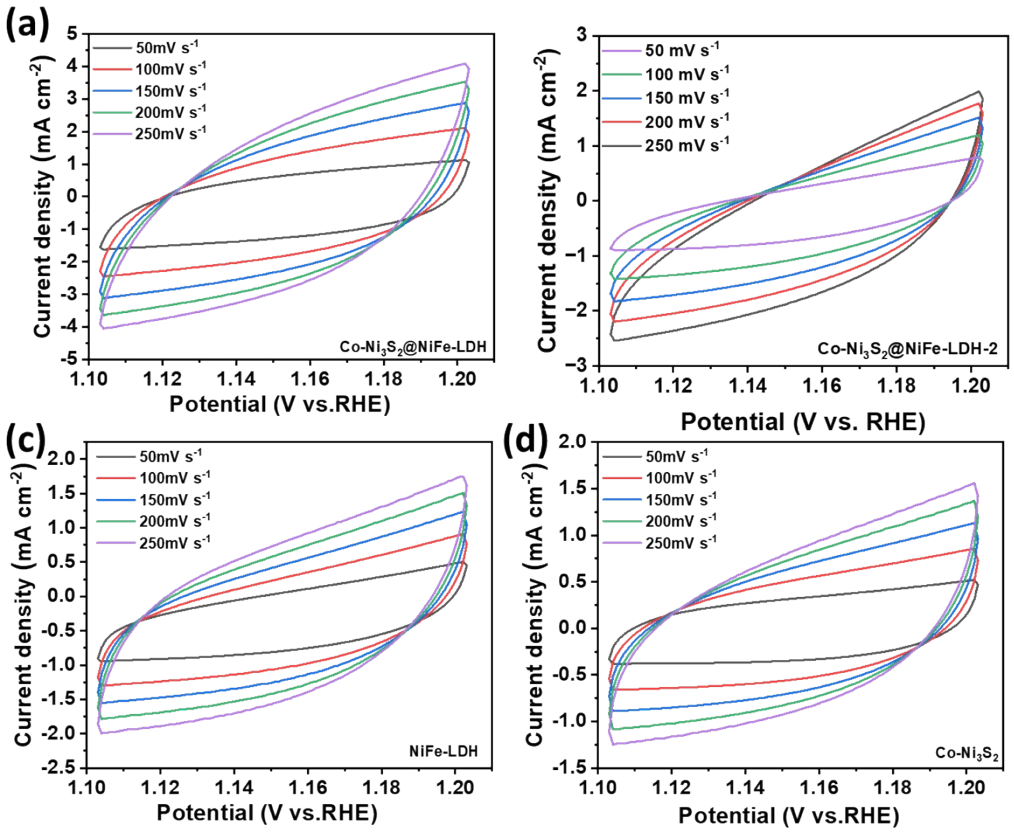

Fig. S6. Cyclic voltammetry curves within the non-Faradaic potential range.

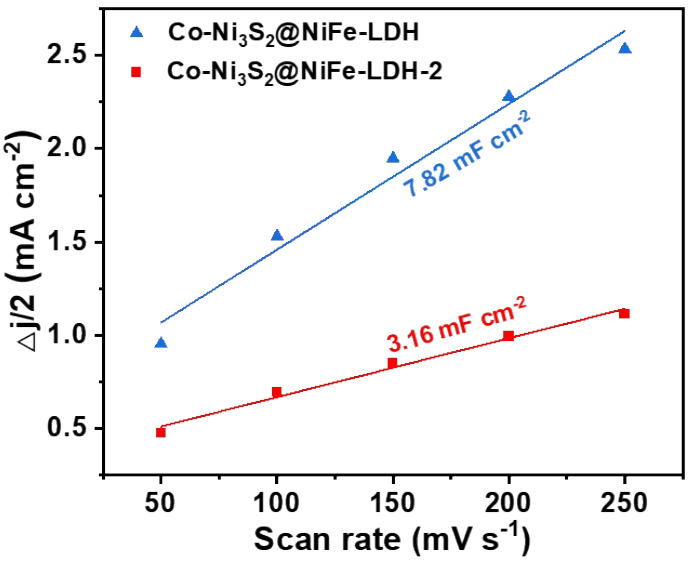

Fig. S7. C_{dl} curves of Co-Ni_3S_2@NiFe-LDH and Co-Ni_3S_2@NiFe-LDH-2.

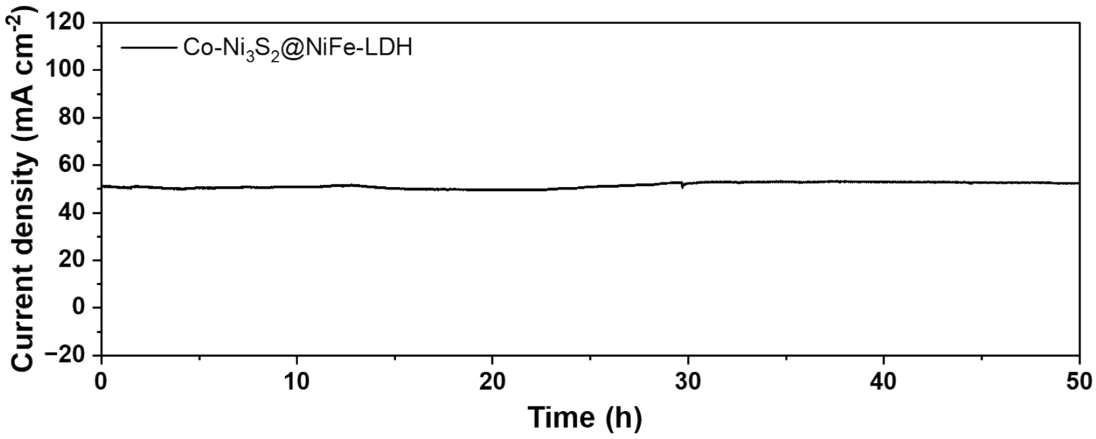

Fig. S8 Stability test of Co-Ni_3S_2@NiFe-LDH at 50 mA cm^{-2}

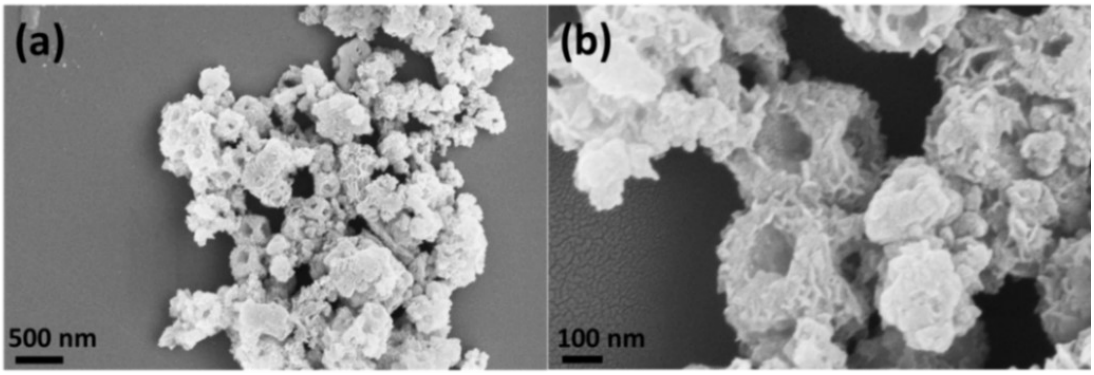

Fig. S9. (a, b) SEM images of Co-Ni_3S_2@NiFe-LDH after OER.

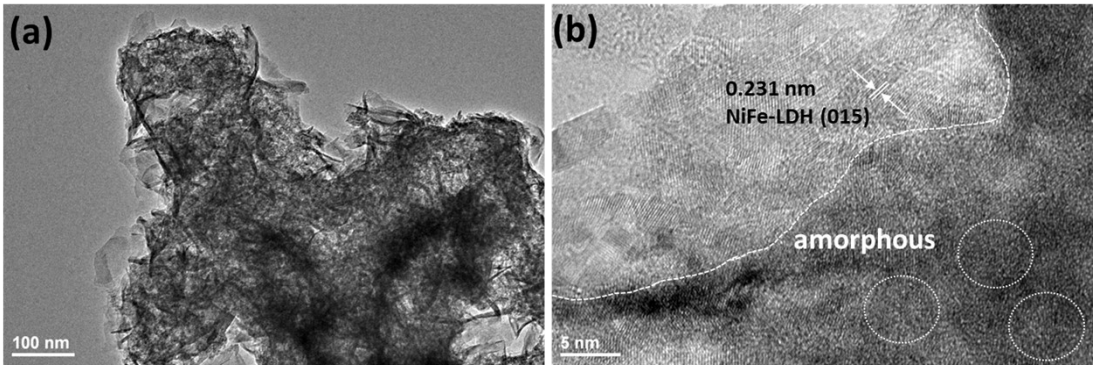

Fig. S10. (a) TEM image and (b) HRTEM image of Co-Ni_3S_2@NiFe-LDH after OER.

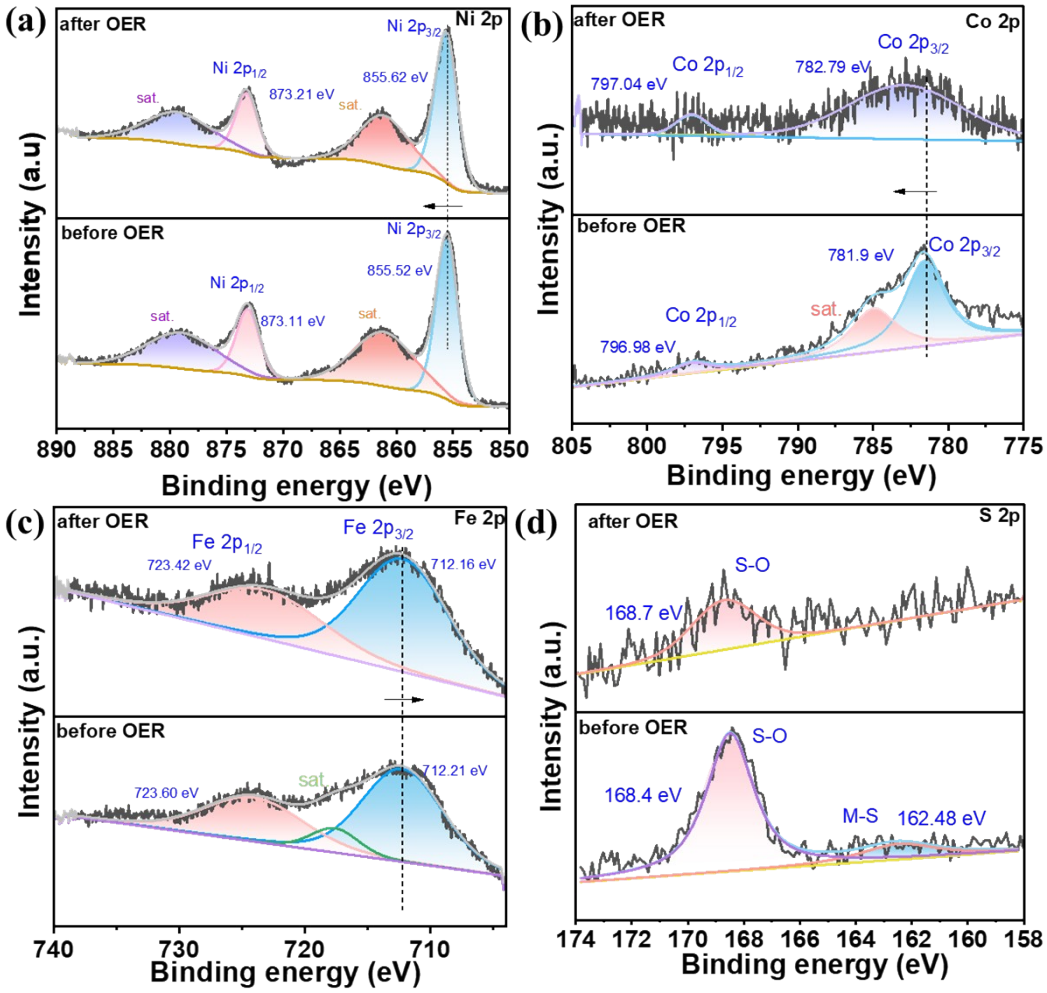

Fig. S11. XPS spectra of (a) Ni 2p, (b) Co 2p, (c) Fe 2p and (d) S 2p in Co-Ni_3S_2@NiFe-LDH before and after OER.

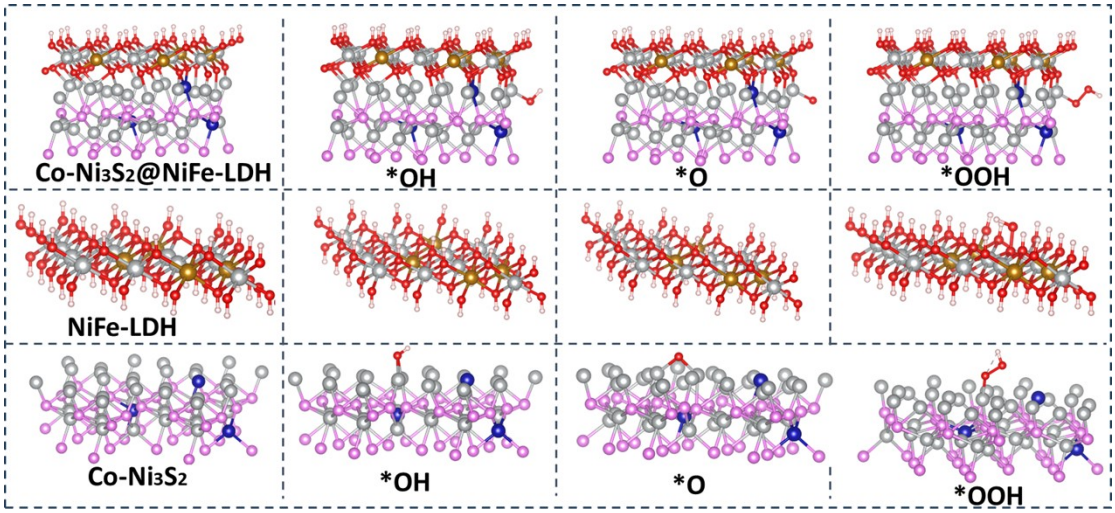

Fig. S12. Theoretical models of Co-Ni_3S_2@NiFe-LDH, Co-Ni_3S_2 and NiFe-LDH for OER in alkaline medium. (Grey: Ni; Purple: S; Blue: Co; Brown: Fe, red: O; Pink: H.)

Table S1.EIS fitting results of NiFe-LDH, Co-Ni_3S_2 and Co-Ni_3S_2@NiFe-LDH

	NiFe-LDH	Co-Ni_3S_2	Co-Ni_3S_2@NiFe-LDH
R_1 (Ω)	1.379	1.353	1.159
R_2 (Ω)	1.619	2.654	0.907

Table S2. Comparison of the OER activities of the Co-Ni_3S_2@NiFe-LDH with some recently-reported catalysts

Catalyst	Electrolyte solution	Overpotential (mV)	Ref.
Co-Ni_3S_2@NiFe-LDH	1.0 M KOH	217 (50 mA cm^{-2})	Our work
$Co_2P_2O_7$@N, P-C	1.0 M KOH	310 (50 mA cm^{-2})	[3]
Co_3O_4/CoS_2	1.0 M KOH	270 (10 mA cm^{-2})	[4]
$Fe_2O_3/ZnCo_2O_4$	1.0 M KOH	261 (10 mA cm^{-2})	[5]
$NiSe_2/FeSe_2$	1.0 M KOH	261 (10 mA cm^{-2})	[6]
MIL-101@NiFe-LDH	1.0 M KOH	215 (20 mA cm^{-2})	[7]
NiFe-LDH/Co_3O_4	1.0 M KOH	274 (50 mA cm^{-2})	[8]
FeCoNi LDH/CuO	1.0 M KOH	243 (50 mA cm^{-2})	[9]
$Co_3O_4/MnCO_3$	1.0 M KOH	273 (10 mA cm^{-2})	[10]
FeOOH/Ni	1.0 M KOH	258.4 (10 mA cm^{-2})	[11]

References

1 G. Kresse and D. Joubert, *Phys. Rev. B*, 1999, **59**, 1758-1775.

2 J. P. Perdew, K. Burke and M. Ernzerhof, *Phys. Rev. Lett.*, 1996, **77**, 3865-3868.

3 D. Liang, C. Lian, Q. Xu, M. Liu, H. Liu, H. Jiang and C. Li, *Appl. Catal., B*, 2020, **268**, 118417.

4 Y. Gao, T. Du, S. Jia, T. Chen, Y. Zhang, F. Yang and X. Zhang, *ChemElectroChem*, 2022, **9**, e202200746.

5 S. Fu, Y. Ma, X. Yang, X. Yao, Z. Jiao, L. Cheng and P. Zhao, *Appl. Catal., B*, 2023, **333**, 122813.

6 S. Ni, H. Qu, Z. Xu, X. Zhu, H. Xing, L. Wang, J. Yu, H. Liu, C. Chen and L. Yang, *Appl. Catal., B*, 2021, **299**, 120638.

7 J. Huang, K. Li, L. Wang, H. She and Q. Wang, *Chin. Chem. Lett.*, 2022, **33**, 3787-3791.

8 Y. Zhang, P. Guo, S. Niu, J. Wu, W. Wang, B. Song, X. Wang, Z. Jiang and P. Xu, *Small Methods*, 2022, **6**, 2200084.

9 Q. Ouyang, S. Cheng, C. Yang and Z. Lei, *J. Mater. Chem. A*, 2022, **10**, 11938-11947.

10 G. Yang, B. Zhu, D. Gao, Y. Fu, J. Zhao and J. Li, *CrystEngComm*, 2020, **22**, 3984-3990.

11 W. Tang, G. Zhang and Y. Qiu, *Int. J. Hydrogen Energy*, 2020, **45**, 28566-28575.